DOI: 10.1002/ejic.200500822

Novel Metallosupramolecular Networks Constructed from Cu^{II}, Ni^{II}, and Cd^{II} with Mixed Ligands: Crystal Structures, Fluorescence, and Magnetism

Miao Du,*[a] Xiu-Juan Jiang,[a] Xiao-Jun Zhao,[a] Hua Cai,[a] and Joan Ribas[b]

Keywords: Coordination polymers / Inclusion complexes / Supramolecular chemistry / Noncovalent interactions

Reactions of mixed ligands succinic acid (H_2suc) and bent dipyridines, such as 2,5-bis(3-pyridyl)-1,3,4-oxadiazole (3-bpo) and its 4-*N*-donor analog (4-bpo), with inorganic Cu^{II}, Ni^{II}, and Cd^{II} salts yield three new metal-organic coordination frameworks $\{[Cu(suc)(3\text{-bpo})(H_2O)_2]\cdot(H_2O)_{1.75}\}_n$ (**1**), $\{[Ni(suc)(4\text{-bpo})(H_2O)_2]\cdot(H_2O)_5\}_n$ (**3**), and $\{[Cd_2(suc)_2(3\text{-bpo})_2(H_2O)_2]\cdot(H_2O)_{6.75}\}_n$ (**4**), in which the metal centers are linked by bridging ligands 3-bpo/4-bpo and suc^{2-} along two directions to form 2D infinite networks. The corrugated 2D nets of **1** and **4**, obtained under hydrothermal conditions, align in an interdigitated manner with the presence of significant aromatic-stacking interactions to result in similar 3D architectures. The 2D sheets in **3** are extended by interlayer hydrogen bonds to afford a 3D structure. However, when succinic acid is replaced by fumaric acid (H_2fum) in the reaction with 3-bpo and Cu^{II} salt, a metallacyclophane $[Cu(Hfum)_2(3\text{-bpo})(H_2O)]_2\cdot(3\text{-bpo})_2\cdot(H_2O)_6$ (**2**) is generated. The binuclear coordinated motifs are hydrogen-bonded to the lattice water chains to furnish a unique 3D channel-like framework, in which the guest 3-bpo molecules are accommodated. The thermal stabilities of these new materials were investigated by thermogravimetric analysis (TGA) of mass loss. The magnetic coupling in complexes **1**–**3** is antiferromagnetic and very small, which is as expected considering the long organic bridges between the paramagnetic centers. The solid-state luminescence properties of **4** reveal an intense fluorescence emission at 378 nm.

Introduction

Research on metal-organic supramolecular chemistry has rapidly developed to produce new materials with interesting structural features and potential applications, and is also one of the most active branches in current coordination chemistry.[1,2] By self-assembly of well-designed organic ligands and metal ions under appropriate conditions, a variety of novel metallosupramolecular architectures, such as coordination polymers and host-guest compounds, have been achieved so far.[1,2] Previous reports have revealed that bifunctional building blocks such as dicarboxylate and dipyridine can bind and bridge metal centers well,[3] and to some extent, it is now possible to predict the target materials based on such ligands containing specific structural and functional information. On the other hand, metal-carboxylate complexes are of great interest in several fields including bioinorganic chemistry,[4] molecular magnetism,[5] and crystal engineering.[6]

Nowadays, the combination of two or more predetermined organic building blocks within a structure has proven to be a powerful synthetic approach to generate functional metal-organic frameworks.[2b,7] Succinic acid (H_2suc) is an effective linking ligand that has been extensively used, together with 4,4′-bipyridine (bipy), to construct mixed-ligand polymeric arrays such as a 1D chain [Zn(suc)(bipy)],[8a] a 3D open framework $[Cu(suc)(bipy)(H_2O)_2]\cdot 2H_2O$,[8a] a 3D pillar-layered network $[Mn(suc)(bipy)(H_2O)]\cdot 0.5bipy$,[8b] a twofold interpenetrated 3D pillar-layered structure $[Cd(suc)(bipy)]\cdot 0.25H_2O$,[8c] and a unique twisting chiral net $[Co(suc)(bipy)(H_2O)_2]\cdot 2H_2O$.[8d] Recently, a dipyridyl *exo*-bidentate heterocyclic ligand, somewhat structurally similar to bipy but with a bent backbone, 2,5-bis(4-pyridyl)-1,3,4-oxadiazole (4-bpo) and its 3-*N*-donor analog (3-bpo) have been involved considerably in our investigations, and a series of interesting discrete/infinite coordination frameworks[9] and organic cocrystalline materials[10] have been generated utilizing their advantage as linking units with the potential ability for coordination, hydrogen-bonding, and/or aromatic-stacking interactions. As an extension of this research, our current work has been focused on simultaneous employment of such N-donor ligands in cooperation with dicarboxylates to assemble new coordination frameworks.[11] In this context, we describe here the preparation, crystal structures, and properties of the mixed-ligand systems $\{[Cu(suc)(3\text{-bpo})(H_2O)_2]\cdot(H_2O)_{1.75}\}_n$ (**1**), $[Cu(Hfum)_2(3\text{-bpo})(H_2O)]_2\cdot(3\text{-bpo})_2\cdot(H_2O)_6$ (**2**), $\{[Ni(suc)(4\text{-bpo})(H_2O)_2]\cdot(H_2O)_5\}_n$ (**3**), and $\{[Cd_2(suc)_2(3\text{-bpo})_2$-

[a] College of Chemistry and Life Science, Tianjin Normal University,
Tianjin 300074, P. R. China
Fax: +86-22-23540315
E-mail: dumiao@public.tpt.tj.cn
[b] Departament de Química Inorgànica, Universitat de Barcelona, Diagonal 647, 08028 Barcelona, Spain

$(H_2O)_2]\cdot(H_2O)_{6.75}\}_n$ (**4**), where H_2fum refers to fumaric acid. Complexes **1**, **3**, and **4** are 2D coordination polymers, while the dinuclear metallacyclophane **2** represents an unusual inclusion compound containing 1D water chains. The magnetic and fluorescence properties of these new materials were also studied.

Results and Discussion

Preparation and Thermal Stabilities of Complexes 1–4

Coordination polymers **1** and **4** were obtained by hydrothermal synthesis, and complexes **2** and **3** were prepared under ambient conditions. In the case of **3**, suitable crystals for X-ray diffraction were achieved by diffusion method in order to facilitate the slow growth of larger single crystals. During the preparation of coordination polymers **1**, **3**, and **4**, the pH environments of the reaction systems were adjusted by triethylamine to promote the complete deprotonation of succinic acid. As a consequence, in the resultant crystalline materials, the succinate dianions act as the bridging blocks to extend the 1D metal-bpo arrays to 2D infinite frameworks. Notably, in the dinuclear complex **2** with the unusual 3D inclusion architecture, the fumaric acid is found in its uncommon mono-deprotonation form and adopts the unprecedented terminal coordination mode with copper. This result is probably related to the fact that the reaction system leading to the generation of **2** does not include a sufficiently strong base. Presumably, the level of deprotonation of the dicarboxylic acid is of great relevance to the final structure of **2**. All complexes are air-stable and insoluble in common organic solvents and water, which is consistent with their polymeric and neutral nature. Thermogravimetric experiments were carried out to explore their thermal stabilities. The TGA curve of **1** shows an obvious weight loss of 6.33% in the range of 46–148 °C (peak: 123 °C), corresponding to the release of the lattice water molecules (calculated: 6.68%). The decomposition of the residuary $[Cu(suc)(3\text{-bpo})(H_2O)_2]$ moiety starts at 187 °C, and then there are three consecutive steps of weight losses ending at 396 °C (peaks: 253, 273, and 358 °C). Further heating to 800 °C reveals no weight loss. Complex **2** remains intact until heating to ca. 100 °C, and then there are three consecutive steps of weight losses (peaks: 182, 260, and 282 °C) concluding at 370 °C. Further heating to 800 °C reveals a continuous and slow weight loss. The TGA curve of **3** suggests that the first weight loss of 17.88% in the range 110–159 °C (peak: 133 °C) corresponds to the expulsion of the lattice water molecules (calculated: 17.14%). Then the coordination framework starts to decompose beyond 195 °C with a series of complicated weight losses, and does not end until heating to 800 °C. For complex **4**, the first step of weight loss (15.59%) in the 62–122 °C range correlates to the elimination of coordinated and lattice water molecules (calculated: 14.82%). The remaining substance does not lose weight upon further heating until two consecutive weight losses (peaks: 276 and 422 °C) occur in the temperature range of 196–478 °C. Further heating to 800 °C reveals no weight loss.

Structural Analysis of Complexes 1–4

{[Cu(suc)(3-bpo)(H$_2$O)$_2$]·(H$_2$O)$_{1.75}$}$_n$ (1)

Single-crystal X-ray diffraction analysis reveals that complex **1** is a 2D metal-organic coordination network in which the metal centers are linked by bidentate suc^{2-} and 3-bpo ligands. Each Cu^{II} atom, located at an inversion center, has an octahedral geometry by virtue of two suc^{2-} oxygen atoms, two 3-bpo nitrogen atoms, and two aqua ligands [Figure 1 (a)], and as expected, the geometry shows Jahn–Teller elongation with two $Cu–O_{water}$ bond distances

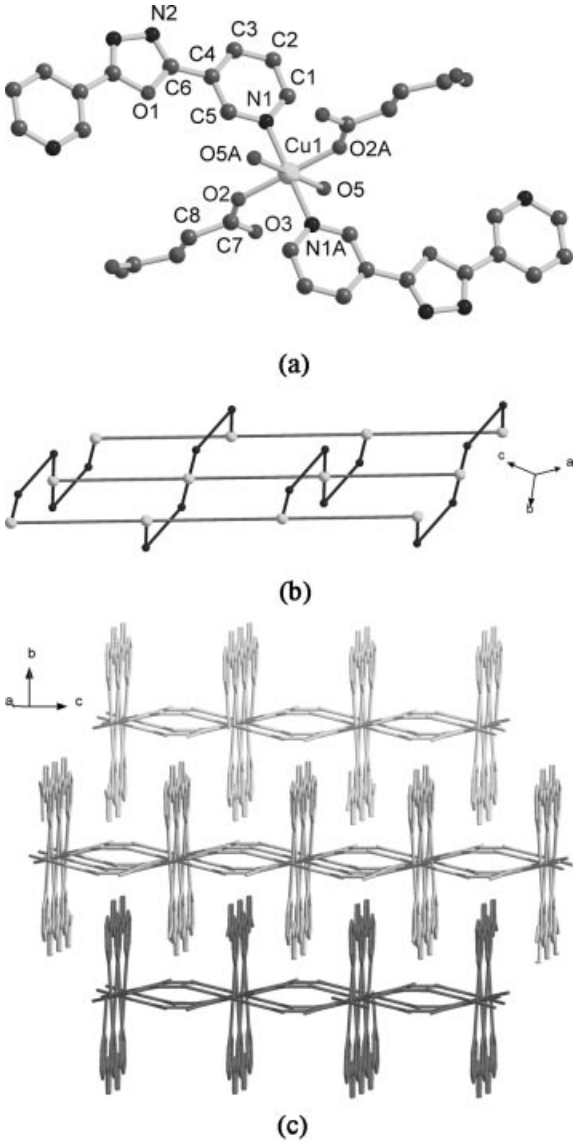

Figure 1. (a) A portion view of **1** with atom labeling of the asymmetric unit and the coordination sphere of copper (all hydrogen atoms are omitted for clarity). (b) A perspective view of the 2D Cu^{II} network with mixed ligands suc^{2-} and 3-bpo, which are simplified as rods and flexuous motifs, respectively. (c) A packing diagram of **1** showing the interdigitation of the 2D networks.

[2.621(7) Å] being significantly longer than those of the other four Cu–O/Cu–N bond lengths [1.947(2)/2.030(3) Å]. The carboxylate group is binding to copper through O(2) in a monodentate fashion, resulting in a longer bond length of C(7)–O(2) than that of C(7)–O(3). Detailed bond parameters are listed in Table 1. Both 3-bpo and suc^{2-} bridging components adopt a *trans* arrangement around copper. As depicted in Figure 1 (b), the 3-bpo molecules connect the Cu^{II} ions to produce a 1D sinusoidal chain, and a similar motif is also observed in $\{[Cu_2(3\text{-bpo})_2(H_2O)_6(SO_4)_2](H_2O)_6\}_n$.[9b] The adjacent chains are arranged in an A(-A) A(-A) sequence and are further interlinked by suc^{2-} ligands in a *trans* bi-monodentate manner to generate a 2D (4,4) network. The distances between the Cu^{II} centers separated by 3-bpo and suc^{2-} are 8.302(3) and 9.499(2) Å, respectively. There also exist intralayer O–H···O hydrogen bonds [O(5)–H(5A)···O(3), H···O and O···O distances: 1.87 and 2.726(4) Å, O–H···O angle: 164°; O(5)–H(5B)···O(3)^{i} (i = $-x + 3/2, -y + 1/2, -z + 1$), H···O and O···O distances: 2.06 and 2.904(5) Å; O–H···O angle: 158°], which further stabilize this framework.

Table 1. Selected bond lengths [Å] and angles [°] for complex **1**.[a]

Bond lengths			
Cu(1)–O(2)	1.947(2)	Cu(1)–N(1)	2.030(3)
Cu(1)–O(5)	2.621(7)	O(2)–C(7)	1.277(4)
O(3)–C(7)	1.231(4)		
Bond angles			
O(2)–Cu(1)–N(1)	89.29(10)	O(2)–Cu(1)–N(1A)	90.71(10)
O(2)–Cu(1)–O(5)	81.51(10)	O(2)–Cu(1)–O(5A)	98.49(10)
N(1)–Cu(1)–O(5A)	87.89(11)	N(1)–Cu(1)–O(5)	92.11(11)

[a] Symmetry codes: A: $-x + 3/2, -y + 1/2, -z$.

The most interesting structural feature of **1** is the packing mode of the 2D networks. As illustrated in Figure 1 (c), the 3-bpo segments lie up and down each 2D sheet, and as a consequence, these 2D arrays are interdigitated with the presence of interlayer π–π stacking interactions between the adjacent 3-bpo molecules. The center-to-center and center-to-plane distances of two antiparallel oxadiazole rings are 4.14 and 3.65 Å, respectively, and those for the pyridyl planes (with a dihedral angle of 4.7°) are 4.15 and 3.70/3.60 Å, respectively. Similar examples with such interdigitation alignment have been documented, which suggest that the stacking interactions can play an important role in extending the structural dimensionality of metallosupramolecular networks.[12]

[Cu(Hfum)$_2$(3-bpo)(H$_2$O)]$_2$·(3-bpo)$_2$·(H$_2$O)$_6$ (2)

When succinic acid was replaced by the more rigid fumaric acid under different reaction conditions, a distinct complex **2** was produced. It consists of a centrosymmetrical binuclear unit $[Cu(Hfum)_2(3\text{-bpo})(H_2O)]_2$, two 3-bpo guests, and lattice water molecules. As shown in Figure 2 (a), in the binuclear entity, each Cu^{II} atom is in a distorted square-pyramidal geometry with a τ parameter of 0.244.[13] Two 3-bpo nitrogen atoms and two carboxylate oxygen atoms of $Hfum^-$ occupy the basal plane, and a water ligand is located at the axial position with a significantly longer Cu–O bond distance of 2.219(3) Å. Selected bond lengths and angles for **2** are listed in Table 2. The two Cu atoms are linked by a pair of 3-bpo molecules to afford a bimetallic ring motif with an intramolecular Cu···Cu distance of 8.385(3) Å. Similar bimetallic macrocycles $[Cu_2(3\text{-bpo})_2(H_2O)_6](ClO_4)_4(H_2O)_4$ and $[Cu(3\text{-bpo})(NO_3)_2]_2(CH_3CN)_2$ were reported recently.[9b] Remarkably, the mono-deprotonated fumaric acid moieties coordinate to Cu^{II} in a unidentate fashion and locate above and below the metallocycle plane. In most documented cases, fumaric acid serves as a dianionic fum bridge using both carboxylate groups,[14] and thus such a unidentate coordination mode of $Hfum^-$ and/or fum^{2-} is quite unique.[15,16] In this structure, as expected, the C–O bonds of the carboxylate groups binding to copper

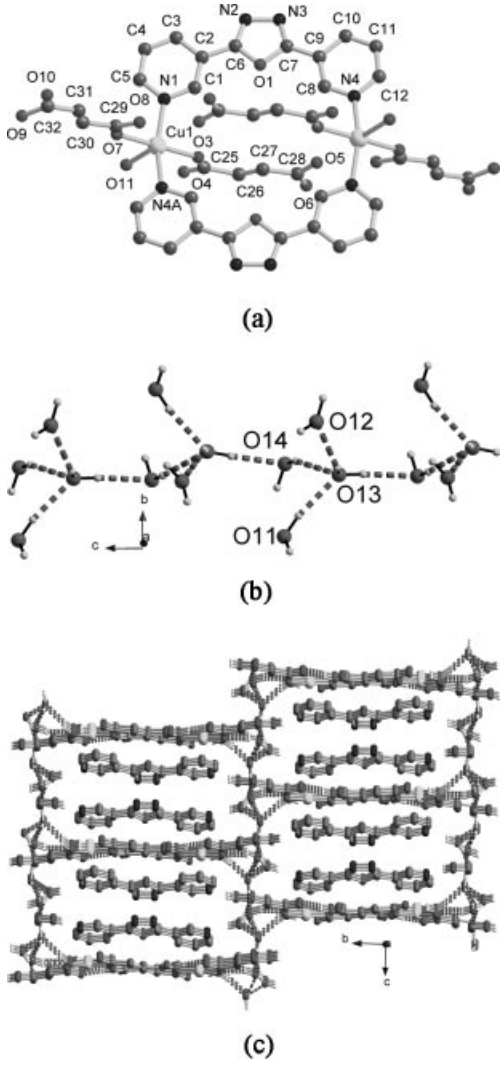

Figure 2. (a) Bimetallic macrocycle of **2** with atom labeling of the asymmetric unit and the coordination sphere of copper (all hydrogen atoms, guest 3-bpo, and lattice water molecules are omitted for clarity). (b) A representation of the 1D water chain linked by water-water interactions. (c) A perspective view of the 3D channel-like hydrogen-bonded network with the accommodation of guest 3-bpo molecules.

have longer lengths than those of the carboxylate groups not binding to copper, and the C–O bonds connecting with the hydrogen atoms of the carboxyl groups are also significant longer (see Table 2 for details). Another unique structural feature of **2** is that the 3-bpo molecules adopt the different *cisoid*-I and *cisoid*-II conformations[9a,17] when present as the bridging ligand and free guest molecule, respectively.

Table 2. Selected bond lengths [Å] and angles [°] for complex **2**.[a]

Bond lengths			
Cu(1)–O(3)	1.935(3)	Cu(1)–O(7)	1.966(3)
Cu(1)–O(11)	2.219(3)	Cu(1)–N(1)	2.043(4)
Cu(1)–N(4A)	2.034(4)	O(3)–C(25)	1.263(5)
O(4)–C(25)	1.231(5)	O(5)–C(28)	1.315(5)
O(6)–C(28)	1.198(5)	O(7)–C(29)	1.263(6)
O(8)–C(29)	1.233(6)	O(9)–C(32)	1.301(6)
O(10)–C(32)	1.204(6)		
Bond angles			
O(3)–Cu(1)–O(7)	176.15(13)	O(3)–Cu(1)–N(4A)	85.93(13)
O(7)–Cu(1)–N(4A)	92.03(13)	O(3)–Cu(1)–N(1)	88.30(13)
O(7)–Cu(1)–N(1)	92.65(13)	N(4A)–Cu(1)–N(1)	161.51(14)
O(3)–Cu(1)–O(11)	95.42(13)	O(7)–Cu(1)–O(11)	88.07(13)
N(4A)–Cu(1)–O(11)	97.64(14)	N(1)–Cu(1)–O(11)	100.39(14)

[a] Symmetry codes: A: $-x$, $1-y$, $1-z$.

Interestingly, the O(14)–H(14B)···O(13) and O(13)–H(13B)···O(14) hydrogen bonds between the lattice water molecules result in the formation of a 1D water chain along the *c* axis [see Figure 2 (b)], around which the lattice O(12) and coordinated O(11) water molecules are fixed by additional O(13)–H(13A)···O(12) and O(11)–H(11B)···O(13) interactions. Detailed hydrogen-bonding geometries are listed in Table 3. The binuclear subunits and the water chains are extended to a 2D layered structure along the crystallographic (011) plane by O(14)–H(14A)···O(7) and above water–water [O(11)···O(13)] interactions, and the structure is also stabilized by the O(11)–H(11A)···O(4) and O(5)–H(5)···O(8) bonds within each binuclear macrocycle. As shown in Figure 2 (c), these 2D arrays are further linked to afford a 3D channel-like network by interlayer O(12)–H(12B)···O(10) interactions, among which the guest 3-bpo entities are accommodated. Hydrogen-bonding interactions such as O(9)–H(9)···N(5) and O(12)–H(12A)···N(8) can be detected between the guest molecules and the host framework. Additionally, significant π–π stacking interactions exist between the adjacent 3-bpo moieties of the dimeric units within each 2D hydrogen-bonded layer, as well as between the neighboring guest 3-bpo molecules located in the cavities, with center-to-center and center-to-face separations of the aromatic rings in the range of 3.27–4.01 and 3.26–3.57 Å, respectively. Presumably, these supramolecular forces could consolidate this interesting host-guest inclusion system.

The significant structural difference between complexes **1** and **2** may be attributed to the intrinsic structural features of the suc^{2-} and $Hfum^{-}$ ligands. We have clearly demonstrated that the structures of Cu^{II} complexes with 3-bpo are solely dependent on the nature of the inorganic counteranions (for example, ClO_4^-, NO_3^-, SO_4^{2-}, and OAc^-),[9b] which afford two types of coordinated motifs such as the 1D sinusoidal chain and binuclear macrocycle (being similar to the cases of **1** and **2**, respectively) when 3-bpo takes the *cisoid*-I conformation. In this work, we can extend this conclusion to organic anions, which are also critical in determining the molecular assembly of the resultant polymeric networks.

{[Ni(suc)(4-bpo)(H$_2$O)$_2$]·(H$_2$O)$_5$}$_n$ (3)

The 2D-layered polymeric network of complex **3** was revealed by X-ray single-crystal diffraction determination. As illustrated in Figure 3 (a), each Ni^{II} center lies on an inversion site and is six-coordinate by binding to a pair of unidentate suc^{2-} ligands, two aqua molecules, and two 4-bpo nitrogen atoms. Important bond lengths and angles are listed in Table 4. Two C–O bond lengths of the monodentate carboxylate group are similar, probably a result of the formation of hydrogen bonds as described later. The octahedral Ni^{II} atoms are interconnected by 4-bpo ligands to afford a wavelike 1D chain running along the crystallographic [010] direction. Adjacent chains are further held together by *trans* bis-monodentate suc dianions, leading to the generation of a 2D undulating (4,4) layer, with the dimensions of the rectangle grid unit of $13.756(1)\times 8.934(1)$ Å^2 [see Figure 3 (b)]. As illustrated in Figure 3 (c), intralayer O(4)–H(4B)···O(3)^{i} (i = $-x$, $-y+1$, $-z+1$) and interlayer O(4)–H(4A)···O(3)^{ii} (ii = $-x+1/2$, $-y+1$, $z-1/2$) interactions between the aqua ligands and uncoordinated carboxylate oxygen atoms are observed.

Table 3. Hydrogen bond geometries in the crystal structure of complex **2**.

D–H···A	D···A [Å]	H···A [Å]	D–H···A [°]	Symmetry codes
O(5)–H(5)···O(8)	2.555(5)	1.74	176	$-x$, $-y+1$, $-z+1$
O(9)–H(9)···N(5)	2.627(5)	1.81	171	
O(11)–H(11A)···O(4)	2.679(5)	1.86	162	
O(11)–H(11B)···O(13)	2.796(6)	1.96	169	$x-1$, y, z
O(12)–H(12A)···N(8)	2.863(6)	2.02	173	$-x+1$, $-y+2$, $-z+1$
O(12)–H(12B)···O(10)	2.967(8)	2.15	160	
O(13)–H(13A)···O(12)	2.697(7)	1.99	140	
O(13)–H(13B)···O(14)	2.803(7)	1.96	175	x, $-y+3/2$, $z+1/2$
O(14)–H(14A)···O(7)	2.864(5)	2.04	164	$x+1$, y, z
O(14)–H(14B)···O(13)	2.815(6)	2.04	152	

These afford two types of 6-membered and 13-membered hydrogen-bonded rings, with H···O/O···O distances of 1.85/2.659(4) and 1.87/2.711(4) Å, respectively, and O–H···O angles of 159 and 170°, respectively. Further analysis of the crystal packing indicates that these 2D waved layers take the parallel stacking mode with some offset, and are further linked to afford a 3D network by interlayer hydrogen bonds as stated earlier. Notably, allowing for the volume of the included disordered water molecules in this 3D open framework, there still remains 190.0 $Å^3$ of void space in the unit cell.[18]

Table 4. Selected bond lengths [Å] and angles [°] for complex **3**.[a]

Bond lengths			
Ni(1)–O(2)	2.024(4)	Ni(1)–O(4)	2.068(3)
Ni(1)–N(1)	2.107(3)	O(2)–C(7)	1.250(5)
O(3)–C(7)	1.244(5)		
Bond angles			
O(2)–Ni(1)–O(4)	87.48(9)	O(4)–Ni(1)–N(1)	93.22(12)
O(2)–Ni(1)–N(1)	88.63(12)	O(2)–Ni(1)–O(4A)	92.52(9)
O(2)–Ni(1)–N(1A)	91.37(12)	O(4)–Ni(1)–N(1A)	86.78(12)

[a] Symmetry codes: A: $-x$, $1-y$, $1-z$.

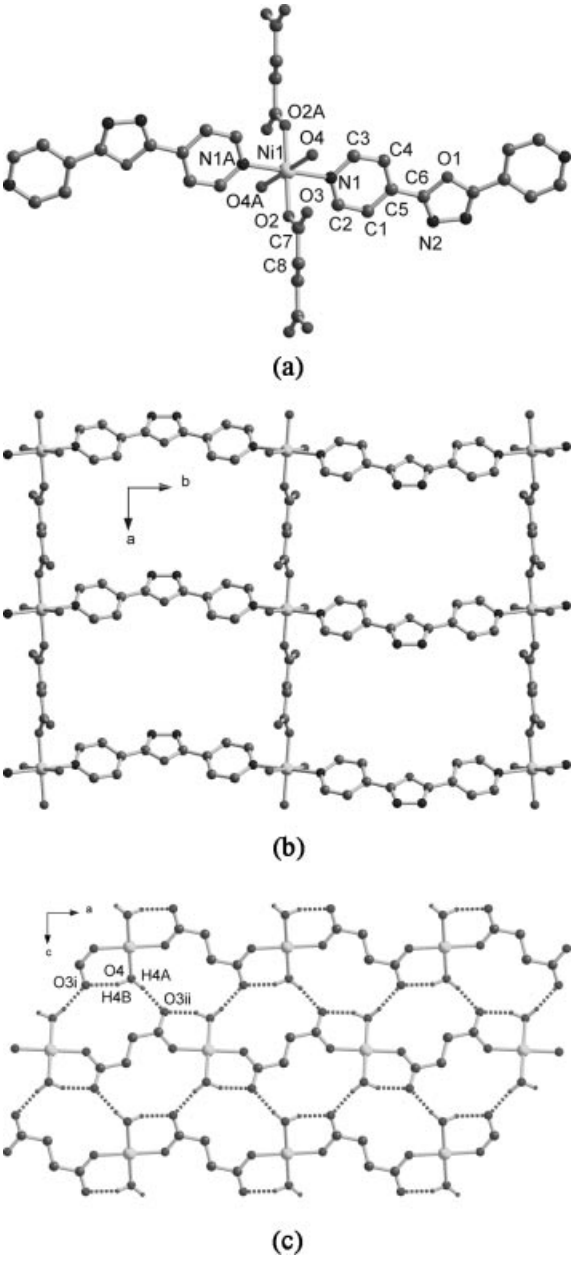

Figure 3. (a) A portion view of **3** with atom labeling of the asymmetric unit and the coordination sphere of nickel (all hydrogen atoms are omitted for clarity). (b) 2D metal-organic network constructed from suc^{2-}/4-bpo and Ni^{II}. (c) A view showing the interlayer and intralayer hydrogen bonds (4-bpo moieties are omitted for clarity).

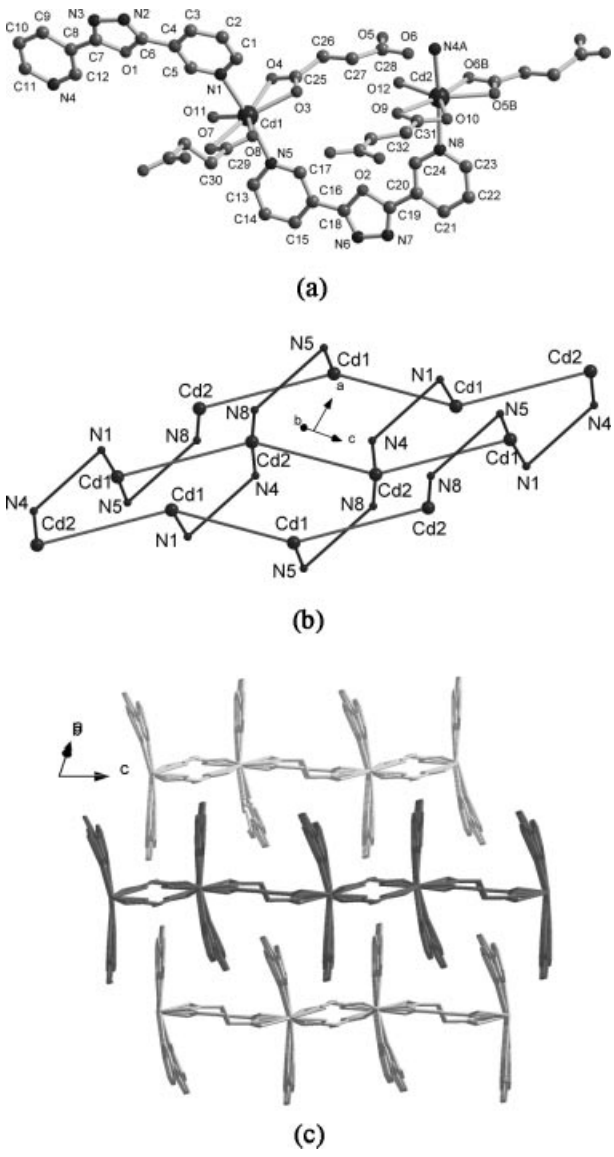

Figure 4. (a) A portion view of **4** with atom labeling of the asymmetric unit and the coordination spheres of cadmium (all hydrogen atoms are omitted for clarity). (b) A perspective view of the 2D Cd^{II} network with mixed ligands suc^{2-} and 3-bpo, which are simplified as rods and flexuous motifs, respectively. (c) A packing diagram of **3** showing the interdigitation of the 2D networks.

{[Cd_2(suc)$_2$(3-bpo)$_2$(H_2O)$_2$]·(H_2O)$_{6.75}$}$_n$ (4)

Complex **4** is also a 2D network, constructed from Cd^{II} and the mixed bridging ligands suc^{2-} and 3-bpo. The local coordination environments around two crystallographically independent Cd^{II} centers are similar, and can be best described as a pentagonal-bipyramidal geometry (CdN_2O_5). The equatorial plane is composed of two chelating carboxylate groups from a pair of suc^{2-} ligands and one oxygen-donor aqua ligand [Cd–O: 2.259(6)–2.485(6) Å], and the axial positions are occupied by two 3-bpo nitrogen atoms [Cd–N: 2.345(8)–2.382(8) Å], as shown in Figure 4 (a). Important bonds lengths and angles are listed in Table 5. Most of the C–O bond lengths of the carboxylate groups are nearly equivalent as a result of their chelated coordination. Similar to the structure of complex **1**, the Cd^{II} ions are connected by 3-bpo and suc^{2-} ligands to furnish a 2D framework with common (4,4) topology [see Figure 4 (b)], and these 2D motifs interdigitate to result in a 3D crystal packing managed by aromatic stacking between 3-bpo moieties [see Figure 4 (c)]. The center-to-center and center-to-face distances between the neighboring 3-bpo molecules are in the range of 3.65–3.78 and 3.35–3.58 Å, respectively. Also, intralayer O(11)–H(11A)···O(4)^i (i = $-x$ + 1, $-y$, $-z$ + 1) and O(12)–H(12B)···O(6) bonds [H···O/O···O distances: 1.95/2.795(9) and 1.89/2.732(8) Å, O–H···O angles: 169 and 172°] can be detected between the aqua ligands and carboxylate groups to further support this structure. However, the arrangement of 3-bpo in **4** is somewhat flexuous, rather than the complanate style as in **1** [see Figure 4 (c)]. This can be attributed to the dissimilar coordination tendency of bpo to Cu^{II} and Cd^{II} metal centers, reflected by the difference in N–M–N angles of 180° for **1** and 168.0(2)/168.1(3)° for **4**.

Table 5. Selected bond lengths [Å] and angles [°] for complex **4**.[a]

Bond lengths			
Cd(1)–O(11)	2.259(6)	Cd(1)–O(3)	2.316(5)
Cd(1)–N(5)	2.345(8)	Cd(1)–N(1)	2.373(8)
Cd(1)–O(7)	2.407(6)	Cd(1)–O(8)	2.436(6)
Cd(1)–O(4)	2.485(6)	Cd(2)–O(12)	2.275(6)
Cd(2)–N(4A)	2.382(8)	Cd(2)–O(5B)	2.343(6)
Cd(2)–N(8)	2.351(7)	Cd(2)–O(10)	2.379(6)
Cd(2)–O(9)	2.390(6)	Cd(2)–O(6B)	2.445(6)
O(3)–C(25)	1.255(9)	O(4)–C(25)	1.251(10)
O(5)–C(28)	1.255(10)	O(6)–C(28)	1.270(10)
O(7)–C(29)	1.251(12)	O(8)–C(29)	1.220(12)
O(9)–C(31)	1.255(11)	O(10)–C(31)	1.266(11)
Bond angles			
O(11)–Cd(1)–O(3)	131.1(2)	O(11)–Cd(1)–N(5)	91.5(3)
O(3)–Cd(1)–N(5)	91.8(2)	O(11)–Cd(1)–N(1)	93.1(3)
O(3)–Cd(1)–N(1)	93.5(3)	N(5)–Cd(1)–N(1)	168.1(3)
O(11)–Cd(1)–O(7)	85.7(2)	O(3)–Cd(1)–O(7)	143.2(2)
N(5)–Cd(1)–O(7)	85.7(2)	N(1)–Cd(1)–O(7)	83.6(3)
O(11)–Cd(1)–O(8)	138.7(2)	O(3)–Cd(1)–O(8)	90.2(2)
N(5)–Cd(1)–O(8)	86.8(3)	N(1)–Cd(1)–O(8)	82.5(3)
O(7)–Cd(1)–O(8)	53.0(2)	O(11)–Cd(1)–O(4)	77.5(2)
O(3)–Cd(1)–O(4)	53.90(19)	N(5)–Cd(1)–O(4)	100.1(2)
N(1)–Cd(1)–O(4)	91.7(3)	O(7)–Cd(1)–O(4)	162.3(2)
O(8)–Cd(1)–O(4)	143.4(2)	O(12)–Cd(2)–O(5B)	133.3(2)
O(12)–Cd(2)–N(8)	93.7(3)	O(5B)–Cd(2)–N(8)	91.9(3)
O(12)–Cd(2)–N(4A)	91.0(3)	O(5B)–Cd(2)–N(4A)	92.9(3)
N(8)–Cd(2)–N(4A)	168.0(2)	O(12)–Cd(2)–O(10)	139.5(2)
O(5B)–Cd(2)–O(10)	87.1(2)	N(8)–Cd(2)–O(10)	86.6(2)
N(4A)–Cd(2)–O(10)	82.7(3)	O(12)–Cd(2)–O(9)	84.6(2)
O(5B)–Cd(2)–O(9)	142.1(2)	N(8)–Cd(2)–O(9)	87.0(3)
N(4A)–Cd(2)–O(9)	82.5(3)	O(10)–Cd(2)–O(9)	55.0(2)
O(12)–Cd(2)–O(6B)	79.0(2)	O(5B)–Cd(2)–O(6B)	54.4(2)
N(8)–Cd(2)–O(6B)	93.0(2)	N(4A)–Cd(2)–O(6B)	98.7(2)
O(10)–Cd(2)–O(6B)	141.5(2)	O(9)–Cd(2)–O(6B)	163.5(2)

[a] Symmetry codes: A: x – 1, y + 1, z; B: $-x$, $-y$ + 1, $-z$ + 1.

A comparison of the three 2D suc/bpo-bridged coordination polymers **1**, **3**, and **4** also reveals the different alignment fashions of the 1D metal–bpo chains. As described earlier, such polymeric chains array in antiparallel [A(-A) A(-A), for **1**] and parallel [AAAA, for **3**] sequences in the resultant 2D networks by further linkage of suc dianions. However, the 1D structures take an A(-A)(-A′)A′ manner in the 2D framework of **4** [see Figure 4 (b)], due to its lower crystallographic symmetry.

Magnetic Properties of Complexes 1–3

The magnetic properties of **1** are shown in Figure 5 (a). The $\chi_M T$ value (χ_M is the molar magnetic susceptibility for one Cu^{II} ion) at 300 K is 0.40 $cm^3 mol^{-1} K$, which is as expected for one magnetically quasi-isolated spin doublet ($g > 2.00$). Starting from room temperature, $\chi_M T$ values smoothly decrease to 50 K and then quickly decrease to 0.09 $cm^3 mol^{-1} K$ at 2 K. The overall trend is characteristic of weak antiferromagnetic interactions. The reduced molar

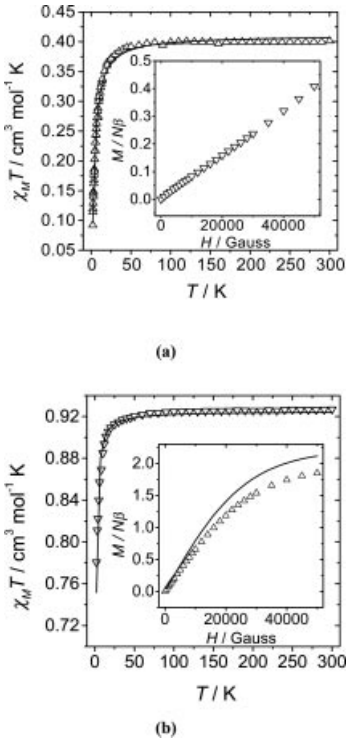

Figure 5. Plot of $\chi_M T$ vs. T for (a) complex **1** and (b) complex **2**. Solid line represents the best fit. Inset: Plot of the reduced magnetization ($M/N\beta$) at 2 K for (a) complex **1** and (b) complex **2** (solid line represents the Brillouin function for g = 2.22).

magnetization at 2 K [see inset in Figure 5 (a)] clearly indicates that the antiferromagnetic coupling is not negligible. The $M/N\beta$ value at 5 T is close to 0.5 electrons and the shape of the curve does not follow the Brillouin law.

Complex **1** is actually a 2D entity in which the Cu^{II} ions are linked by suc^{2-} and 3-bpo ligands. Both ligands are very long, and thus a small antiferromagnetic coupling is expected. Layers can be considered as pseudoquadratic. Considering these structural features, we have fitted the susceptibility data by the expression given by Rushbrooke and Wood for a Heisenberg square-planar system.[19] The expression was deduced by taking into account the $S = ½$ value for the Cu^{II} ion, based on the spin Hamiltonian $H = -2J\Sigma_{ij}S_iS_j$.

$$\chi_M T = \frac{Ng^2\beta^2}{4k}\left[1-\frac{2}{x}+\frac{2}{x^2}-\frac{1.333}{x^3}+\frac{0.25}{x^4}+\frac{0.4833}{x^5}+\frac{0.003797}{x^6}\right]^{-1}$$

In this expression $x = kT/J$, and N, β, and k have the usual meanings. The values obtained for the exchange parameters are $J = -1.06 \pm 0.01$ cm^{-1}, $g = 2.10 \pm 0.01$, and $R = 4 \times 10^{-5}$ (R is the agreement factor defined as $\Sigma_i[(\chi_M T)_{obs} - (\chi_M T)_{calc}]^2/\Sigma[(\chi_M T)_{obs}]^2$ in this and the subsequent cases). This small J value can be interpreted as a consequence of the weak overlap between the Cu^{II} ions through the long organic ligands.

The magnetic properties of **2** as a $\chi_M T$ versus T plot (χ_M is the molar magnetic susceptibility for two Cu^{II} ions) and the reduced magnetization ($M/N\beta$ versus H, inset) are shown in Figure 5 (b). The value of $\chi_M T$ at 300 K is 0.93 cm^3 mol^{-1} K, which is as expected for two isolated Cu^{II} ions without coupling ($g > 2.00$). Starting from room temperature, $\chi_M T$ values are practically constant to 50 K, and below 50 K they quickly decrease to 0.78 cm^3 mol^{-1} K at 2 K. This feature is characteristic of very weak antiferromagnetic interactions between the Cu^{II} ions, which is also clearly corroborated by the reduced molar magnetization at 2 K. The $M/N\beta$ value at 5 T is close to 1.8 electrons and the curve is below the theoretical Brillouin function for $g = 2.22$. The fit of the susceptibility data of the dinuclear Cu^{II} complex **2** was carried out by application of the Bleaney–Bowers formula.[20] The best-fit parameters obtained are $J = -0.90 \pm 0.01$ cm^{-1}, $g = 2.22 \pm 0.01$, and $R = 6.1 \times 10^{-5}$. The small J value can be interpreted as a consequence of the almost nil overlap between the two Cu^{II} ions through the long 3-bpo bridging ligand.[9]

On comparison of the $\chi_M T$ curves for complexes **1** and **2**, it is worth noting their quite different scales [see Figure 5 (a) and (b), respectively]. The $\chi_M T$ range (300–2 K) for **1** is approximately 0.4 to 0.1 cm^3 mol^{-1} K, whereas the range for **2** is only 0.93 to 0.78 cm^3 mol^{-1} K. This feature corresponds to the different behaviors of the reduced magnetization for both complexes, indicating that the antiferromagnetic coupling is smaller in complex **2**.

The plot of $\chi_M T$ versus T for one Ni^{II} ion (complex **3**) is shown in Figure 6 (a). From room temperature to 50 K, $\chi_M T$ values are constantly close to ca. 1.20 cm^3 mol^{-1} K, which is typical for one isolated Ni^{II} ion with $g > 2.00$. There is a small decrease down to 40 K, and then to 0.75 cm^3 mol^{-1} K at 2 K, indicating a very small antiferromagnetic coupling or the logical existence of the zero-field splitting (ZFS) of Ni^{II} ions. The plot of the reduced magnetization ($M/N\beta$) for **3** is also shown in the inset in Figure 6 (a). The expected value of reduced magnetization for two unpaired electrons at saturation would be 2.3 (assuming $g = 2.15$, which is the g value obtained from magnetic measurements, see later). The experimental value is close to 1.8 electrons at 2 K and 50000 Gauss. In the same figure we have represented the Brillouin function for $S = 1$ and $g = 2.15$. The experimental data are below the theoretical curve, indicating either the presence of weak antiferromagnetic interactions or, most likely, the signature of single-ion ZFS (D) of Ni^{II}.

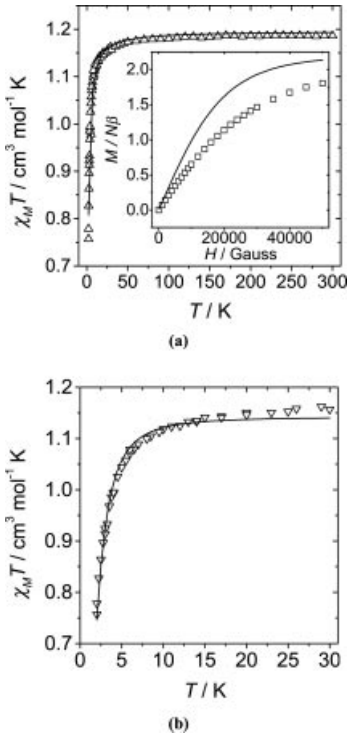

Figure 6. (a) Plot of $\chi_M T$ vs. T for complex **3**. Solid line represents the best fit. Inset: Plot of the reduced magnetization ($M/N\beta$) at 2 K (solid line represents the Brillouin function at 2 K for $g = 2.15$). (b) Plot of the low temperature $\chi_M T$ region, assuming isolated Ni^{II} ions with zero-field splitting (D parameter). Solid line represents the best fit.

The structure of **3** is also a 2D case, which is difficult to fit, mainly due to small J values. Therefore, in the first approach, we can assume that the long 3-bpo ligand does not create any coupling, and thus the small experimental coupling is due to the suc^{2-} ligand. With this hypothesis, we can assume that complex **3** behaves as a 1D system. For systems of this kind, isotropic 1D $S = 1$, the temperature-dependence of the susceptibility extrapolated from calculations performed on ring systems of increasing length has been given by Weng,[21] which is valid only for antiferromagnetic coupling. Neither ZFS nor the Haldane gap effect[22] is taken into account in this expression. The best-fit parameters for **3** are $J = -0.38 \pm 0.01$ cm^{-1}, $g = 2.14 \pm 0.01$,

and $R = 2.0 \times 10^{-4}$. As indicated earlier, the small decrease in $\chi_M T$ values from 40 to 2 K could also be attributed to the typical single-ion ZFS for isolated Ni^{II} ions, which is usually very great and of the order of 4–6 cm^{-1}.[23] For this reason we have also fitted the low temperature region assuming isolated Ni^{II} ions (without any coupling), applying the formula given by Kahn for this $S = 1$ case.[20] It is important to emphasize that with this method it is only possible to calculate the absolute value of D, that is $|D|$, not its sign.[20] With this hypothesis, the best fit was obtained with the parameters $|D| = 3.9\ cm^{-1}$ and $g = 2.14$ [see Figure 6 (b)]. The calculated D value lies in the order of magnitude typical for isolated Ni^{II} ions, as indicated earlier.[23]

As a conclusion, we must emphasize that the two phenomena (small coupling and single-ion ZFS) may be active in this type of nickel complex. It is impossible to separate both components with these standard measurements. In any case, the antiferromagnetic coupling must be very small, as expected for the length of the bridging ligands.

Luminescence Study of Complex 4

Solid-state luminescence properties of the polymeric Cd^{II} (d^{10} metal) complex **4** with the aromatic ligand 3-bpo were investigated ($\lambda_{ex} = 320$ nm). The free 3-bpo molecule displays an emission maximum at 364 nm, whereas a broad and intense emission band at 378 nm is observed for complex **4**. Hence, the fluorescence wavelength of 3-bpo is considerably affected by the incorporation of metal-coordination interactions. This significant red-shift phenomenon may be assigned to the ligand-to-metal charge transfer (LMCT). The intense fluorescence emission also shows that the coordination polymer **4** could have roles as potential photoactive inorganic-organic hybrid material.

Conclusions

Three 2D metal-organic coordination polymers and a unique 3D metallosupramolecular inclusion complex have been achieved through self-assembly of metal ions and mixed organic ligands under different conditions. These new crystalline materials also display such useful properties as magnetism and fluorescence. This study clearly indicates that 3-bpo/4-bpo and suc^{2-} ligands could act as excellent bridging spacers to construct programmed coordination polymers, and such a mixed-ligand synthetic strategy may further flourish this attractive chemistry. Further studies of the design and preparation of new metal-organic coordination frameworks with the bent *exo*-dipyridyl building blocks and other organic carboxylic acids (for example, the commonly used terephthalic, trimesic, and pyromellitic acids) are underway in our laboratory.

Experimental Section

General Materials and Methods: All the reagents and solvents for synthesis and analysis were commercially available and used as received, except for 3-bpo and 4-bpo, which were prepared according to literature procedures.[24] FTIR spectra (KBr pellets) were recorded with an AVATAR-370 (Nicolet) spectrometer. Carbon, hydrogen, and nitrogen analyses were performed with a CE-440 (Leemanlabs) analyzer. TGA experiments were carried out with a Dupont thermal analyzer from room temp. to 800 °C under nitrogen at a heating rate of 10 °C/min. Fluorescence spectra were recorded with a Cary Eclipse spectrofluorimeter (Varian) equipped with a xenon lamp and quartz carrier at room temp.

Magnetic Studies: The variable-temp. magnetic susceptibilities were measured in the "Servei de Magnetoquímica (Universitat de Barcelona)" on polycrystalline samples (30 mg) with a Quantum Design SQUID MPMS-XL susceptometer, operating in the temp. range of 2–300 K and a magnetic field of 0.1 T. The diamagnetic corrections were evaluated from Pascal's constants for all constituent atoms.

Syntheses of the Complexes

$\{[Cu(suc)(3\text{-bpo})(H_2O)_2]\cdot(H_2O)_{1.75}\}_n$ (1): A mixture of succinic acid (17.2 mg, 0.15 mmol), $Cu(OAc)_2\cdot H_2O$ (23.5 mg, 0.12 mmol), 3-bpo (26.4 mg, 0.12 mmol), and triethylamine (0.2 mL) in water (10 mL) was sealed in a Teflon-lined stainless steel vessel (20 mL), which was heated at 140 °C for 5 d and then cooled to room temp. at a rate of 5 °C/h. Blue prism crystals were collected in 42% yield (24.0 mg, based on 3-bpo). $C_{16}H_{19.5}CuN_4O_{8.75}$ (471.40): calcd. C 40.76, H 4.17, N 11.88; found C 40.50, H 3.55, N 11.47. IR (KBr): $\tilde{\nu}$ = 3407 (br), 1616 (vs), 1556 (vs), 1482 (s), 1417 (vs), 1390 (vs), 1338 (s), 1284 (m), 1230 (s), 1194 (m), 1127 (m), 1083 (m), 1052 (m), 964 (m), 825 (s), 732 (s), 690 (vs) cm^{-1}.

$[Cu(Hfum)_2(3\text{-bpo})(H_2O)]_2\cdot(3\text{-bpo})_2\cdot(H_2O)_6$ (2): A mixture of fumaric acid (59.6 mg, 0.51 mmol) and $Cu(OAc)_2\cdot H_2O$ (38.9 mg, 0.19 mmol) in CH_3OH/H_2O (10 mL, v:v = 1:1) was stirred for 10 min and the resultant blue precipitate was filtered. A solution of 3-bpo (23.6 mg, 0.10 mmol) in CH_3OH (10 mL) was added to the filtrate with constant stirring for 30 min and then left to stand at room temp., producing blue block crystals after a period of 1 week in 12% yield (5.1 mg, based on 3-bpo). $C_{64}H_{60}Cu_2N_{16}O_{28}$ (1628.36): calcd. C 47.20, H 3.71, N 13.76; found C 47.42, H 3.84, N 13.72. IR (KBr): $\tilde{\nu}$ = 3432 (s), 3074 (s), 1720 (s), 1600 (vs), 1481 (m), 1413 (s), 1390 (vs), 1330 (s), 1282 (vs), 1251 (s), 1201 (s), 1164 (s), 1081 (m), 1042 (m), 975 (s), 829 (m), 730 (s), 695 (vs), 652 (s) cm^{-1}.

$\{[Ni(suc)(4\text{-bpo})(H_2O)_2]\cdot(H_2O)_5\}_n$ (3): The pH of a CH_3OH/H_2O (5 mL, v:v = 1:1) solution containing succinic acid (14.5 mg, 0.12 mmol) and $Ni(ClO_4)_2\cdot 6H_2O$ (47.5 mg, 0.13 mmol) was adjusted to 7 with triethylamine. The resultant mixture was then carefully layered onto a buffer of glycol (2 mL), below which a solution of 4-bpo (23.4 mg, 0.11 mmol) in $CHCl_3$ (2 mL) was placed in a straight glass tube. Upon slow evaporation of the solvents over 2 weeks, green lamellar single crystals suitable for X-ray analysis were obtained in 26% yield (15.0 mg, based on 4-bpo). $C_{16}H_{26}N_4NiO_{12}$ (525.12): calcd. C 36.59, H 4.99, N 10.67; found: C 35.98, H 4.07, N 11.15. IR (KBr): $\tilde{\nu}$ = 3100 (br), 1546 (vs), 1489 (s), 1420 (vs), 1278 (w), 1224 (m), 1120 (w), 1063 (m), 1017 (w), 970 (w), 842 (s), 753 (s), 716 (s), 677 (s), 511 (m) cm^{-1}.

$\{[Cd_2(suc)_2(3\text{-bpo})_2(H_2O)_2]\cdot(H_2O)_{6.75}\}_n$ (4): The same hydrothermal procedure as for **1** was used except that $Cu(OAc)_2\cdot H_2O$ was replaced by $Cd(OAc)_2\cdot 2H_2O$, affording colorless block crystals of **4** in 58% yield (37.2 mg, based on 3-bpo). $C_{32}H_{41.5}Cd_2N_8O_{18.75}$ (1063.03): calcd. C 36.15, H 3.94, N 10.54; found: C 35.55, H 4.04, N 10.04. IR (KBr): $\tilde{\nu}$ = 3412 (br), 1581 (vs), 1548 (s), 1466 (m), 1415 (vs), 1292 (s), 1233 (w), 1192 (m), 1084 (m), 1029 (m), 900 (m), 815 (m), 732 (s), 692 (s), 639 (m) cm^{-1}.

Table 6. Crystallographic data and structure refinement summary for complexes **1**–**4**.

	1	**2**	**3**	**4**
Empirical formula	$C_{16}H_{19.5}CuN_4O_{8.75}$	$C_{64}H_{60}Cu_2N_{16}O_{28}$	$C_{16}H_{26}N_4NiO_{12}$	$C_{32}H_{41.5}Cd_2N_8O_{18.75}$
Mr	471.40	1628.36	525.12	1063.03
Crystal size [mm]	0.22×0.20×0.16	0.24×0.20×0.12	0.49×0.30×0.08	0.20×0.16×0.14
Crystal system	monoclinic	monoclinic	orthorhombic	triclinic
Space group	*C*2/*c*	$P2_1/c$	*Pnma*	$P\bar{1}$
a [Å]	16.031(6)	12.576(4)	8.9342(9)	11.971(4)
b [Å]	16.249(6)	32.497(11)	27.512(3)	13.116(4)
c [Å]	7.829(3)	9.226(3)	11.7133(12)	15.075(5)
α [°]	90	90	90	75.672(5)
β [°]	99.777(6)	107.843(6)	90	77.826(5)
γ [°]	90	90	90	88.422(6)
V [Å^3]	2009.7(13)	3589(2)	2879.1(5)	2241.0(13)
Z	4	2	4	2
D_c [g cm^{-3}]	1.558	1.507	1.211	1.575
μ [mm^{-1}]	1.142	0.689	0.728	1.028
F(000)	970	1676	1096	1071
Total/independent Reflections	5148/1783	18445/6309	14632/2601	11725/7874
Parameters	148	498	204	586
R_{int}	0.0360	0.0673	0.0251	0.0393
R,[a] R_w[b]	0.0437, 0.0982	0.0575, 0.1272	0.0530, 0.1840	0.0536, 0.1328
GOF[c]	1.115	1.108	1.080	1.028
Residuals [e Å^{-3}]	0.374, –0.310	0.515, –0.396	0.761, –0.430	0.941, –0.555

[a] $R = \Sigma||F_o| - |F_c||/\Sigma|F_o|$. [b] $R_w = [\Sigma[w(F_o^2 - F_c^2)^2]/\Sigma w(F_o^2)^2]^{1/2}$. [c] GOF = $\{\Sigma[w(F_o^2 - F_c^2)^2]/(n - p)\}^{1/2}$.

Caution! Perchlorate complexes of metal ions in the presence of organic ligands are potentially explosive. Only a small amount of material should be handled and with care.

X-ray Crystallography: Single-crystal X-ray diffraction data for complexes **1**–**4** were collected with a Bruker Apex II CCD diffractometer at 293(2) K with Mo-*Kα* radiation (λ = 0.71073 Å) by ω scan mode. There was no evidence of crystal decay during data collection. A semiempirical absorption correction was applied using the SADABS program, and the program SAINT was used for integration of the diffraction profiles.[25] The structures were solved by direct methods using the SHELXS program of the SHELXTL package and refined with SHELXL.[26] The final refinement was performed by full-matrix least-squares methods with anisotropic thermal parameters for all non-hydrogen atoms on F^2. Hydrogen atoms bonded to carbon were placed geometrically and allowed to ride during subsequent refinement with an isotropic displacement parameter fixed at 1.2 times U_{eq} of the parent atoms. Hydrogen atoms of the aqua ligands in all structures and the lattice water molecules in **2** were first located in difference Fourier maps, and then placed at calculated positions and included in the final refinement. The lattice water in the structures of **1**, **3**, and **4** were treated using the disordered model and their hydrogen atoms not located. Starting positions for carboxyl hydrogen atoms in the structure of **2** were located in difference syntheses, and refinement was performed using rigid O–H groups allowed to rotate but not tip, with the bond length of 0.82 Å. Further crystallographic data and structure refinement parameters of complexes **1**–**4** are summarized in Table 6.

CCDC-284066 to -284069 (for **1**–**4**, respectively) contain the supplementary crystallographic data for this paper. These data can be obtained free of charge from The Cambridge Crystallographic Data Centre via www.ccdc.cam.ac.uk/data_request/cif.

Acknowledgments

This work was financially supported by the National Natural Science Foundation of China (No. 20401012), the Key Project of Tianjin Natural Science Foundation (No. 043804111), and Tianjin Normal University. J. R. acknowledges the financial support from the Spanish Government (Grant BQU2003/00539).

[1] a) M. W. Hosseini, *Acc. Chem. Res.* **2005**, *38*, 313–323; b) S. Kitagawa, R. Kitaura, S. Noro, *Angew. Chem. Int. Ed.* **2004**, *43*, 2334–2375; c) L. Carlucci, G. Ciani, D. M. Proserpio, *Coord. Chem. Rev.* **2003**, *246*, 247–289; d) O. R. Evans, W. B. Lin, *Acc. Chem. Res.* **2002**, *35*, 511–522; e) B. Moulton, M. J. Zaworotko, *Chem. Rev.* **2001**, *101*, 1629–1658.

[2] a) P. J. Steel, *Acc. Chem. Res.* **2005**, *38*, 243–250; b) B. H. Ye, M. L. Tong, X. M. Chen, *Coord. Chem. Rev.* **2005**, *249*, 545–565; c) L. Brammer, *Chem. Soc. Rev.* **2004**, *33*, 476– 489; d) C. Janiak, *Dalton Trans.* **2003**, 2781–2804; e) S. R. Seidel, P. J. Stang, *Acc. Chem. Res.* **2002**, *35*, 972–983; f) D. L. Caulder, K. N. Raymond, *Acc. Chem. Res.* **1999**, *32*, 975–982.

[3] a) Y. J. Kim, E. W. Lee, D.-Y. Jung, *Chem. Mater.* **2001**, *13*, 2684–2690; b) Y. J. Kim, M. K. Suh, D.-Y. Jung, *Inorg. Chem.* **2004**, *43*, 245–250; c) S. A. Barnett, N. R. Champness, *Coord. Chem. Rev.* **2003**, *246*, 145–168; d) S. Noro, R. Kitaura, M. Kondo, S. Kitagawa, T. Ishii, H. Matsuzaka, M. Yamashita, *J. Am. Chem. Soc.* **2002**, *124*, 2568–2583.

[4] a) D. Lee, B. Pierce, C. Krebs, M. P. Hendrich, B. H. Huynh, S. J. Lippard, *J. Am. Chem. Soc.* **2002**, *124*, 3993–4007; b) E. L. Hegg, R. Y. N. Ho, L. Que, Jr., *J. Am. Chem. Soc.* **1999**, *121*, 1972–1973; c) J. B. Vincent, G. L. Olivier-Lilley, B. A. Averill, *Chem. Rev.* **1990**, *90*, 1447–1467; d) G. Christou, *Acc. Chem. Res.* **1989**, *22*, 328–335.

[5] a) F. S. Delgado, J. Sanchiz, C. Ruiz-Perez, F. Lloret, M. Julve, *Inorg. Chem.* **2003**, *42*, 5938–5948; b) W. Wernsdorfer, N. Aliaga-Alcalde, D. N. Hendrickson, G. Christou, *Nature* **2002**, *416*, 406–409; c) J. T. Brockman, J. C. Huffman, G. Christou, *Angew. Chem. Int. Ed.* **2002**, *41*, 2506–2508; d) D. Gatteschi, A. Caneschi, L. Pardi, R. Sessoli, *Science* **1994**, *265*, 1054–1058.

[6] a) O. M. Yaghi, M. O'Keeffe, N. W. Ockwig, H. K. Chae, M. Eddaoudi, J. Kim, *Nature* **2003**, *423*, 705–714; b) C. N. R. Rao, S. Natarajan, R. Vaidhyanathan, *Angew. Chem. Int. Ed.* **2004**, *43*, 1466–1496.

[7] a) J. Tao, M. L. Tong, X. M. Chen, *J. Chem. Soc., Dalton Trans.* **2000**, 3669–3674; b) X. J. Li, R. Cao, D. F. Sun, W. H.

Bi, Y. Q. Wang, X. Li, M. C. Hong, *Cryst. Growth Des.* **2004**, *4*, 775–780; c) J. Tao, Y. Zhang, M. L. Tong, X. M. Chen, T. Yuen, C. L. Lin, X. Y. Huang, J. Li, *Chem. Commun.* **2002**, 1342–1343.

[8] a) S. M. Ying, J. G. Mao, Y. Q. Sun, H. Y. Zeng, Z. C. Dong, *Polyhedron* **2003**, *22*, 3097–3103; b) Y. Q. Zheng, J. L. Lin, Z. P. Kong, *Inorg. Chem.* **2004**, *43*, 2590–2596; c) J. Zhang, Z.-J. Li, Y.-H. Wen, Y. Kang, J.-K. Cheng, Y.-G. Yao, *Z. Anorg. Allg. Chem.* **2004**, *630*, 2731–2735; d) J. Zhang, Y. Kang, R.-B. Zhang, Z.-J. Li, J.-K. Cheng, Y.-G. Yao, *CrystEngCommun.* **2005**, *7*, 177–178.

[9] a) M. Du, X.-H. Bu, Y.-M. Guo, H. Liu, S. R. Batten, J. Ribas, T. C. W. Mak, *Inorg. Chem.* **2002**, *41*, 4904–4908; b) M. Du, X.-H. Bu, Z. Huang, S.-T. Chen, Y.-M. Guo, C. Diaz, J. Ribas, *Inorg. Chem.* **2003**, *42*, 552–559; c) M. Du, Y.-M. Guo, S.-T. Chen, X.-H. Bu, S. R. Batten, J. Ribas, S. Kitagawa, *Inorg. Chem.* **2004**, *43*, 1287–1293.

[10] a) M. Du, Z.-H. Zhang, X.-J. Zhao, *Cryst. Growth Des.* **2005**, *5*, 1199–1208; b) M. Du, Z.-H. Zhang, X.-J. Zhao, *Cryst. Growth Des.* **2005**, *5*, 1247–1254; c) M. Du, Z.-H. Zhang, X.-J. Zhao, H. Cai, *Cryst. Growth Des.* **2006**, *6*, 114–121.

[11] a) M. Du, H. Cai, X.-J. Zhao, *Inorg. Chim. Acta* **2005**, *358*, 4034–4038; b) M. Du, H. Cai, X.-J. Zhao, *Inorg. Chim. Acta* **2005**, 673–679.

[12] a) L. Y. Zhang, G. F. Liu, S. L. Zheng, B. H. Ye, X. M. Zhang, X. M. Chen, *Eur. J. Inorg. Chem.* **2003**, 2965–2971; b) D. Q. Chu, J. Q. Xu, L. M. Duan, T. G. Wang, A. Q. Tang, L. Ye, *Eur. J. Inorg. Chem.* **2001**, 1135–1137.

[13] A. W. Addison, T. N. Rao, J. Reedijk, J. Van Rijn, G. C. Verschoor, *J. Chem. Soc., Dalton Trans.* **1984**, 1349–1356.

[14] a) A. Michaelides, S. Skoulika, M. G. Siskos, *Chem. Commun.* **2004**, 2418–2419; b) S. Konar, E. Zangrando, N. R. Chaudhuri, *Inorg. Chim. Acta* **2003**, *355*, 264–271; c) A. Michaelides, S. Skoulika, M. G. Siskos, *Chem. Commun.* **2001**, 1346–1347; d) J. Tao, M. L. Tong, J. X. Shi, X. M. Chen, S. W. Ng, *Chem. Commun.* **2000**, 2043–2044.

[15] Unidentate coordination of $Hfum^-$ is unprecedented; for unidentate coordination of $Hmal^-$ (mal = maleate dianion) using its carboxylate oxygen see: a) A. Sequeira, H. Rajagopal, M. P. Gupta, F. Vanhouteghem, A. T. H. Lenstra, H. J. Geise, *Acta Crystallogr. Sect. C: Cryst. Struct. Commun.* **1992**, *48*, 1192–1197. For unidentate coordination of $Hmal^-$ using its carboxyl oxygen (notably, both cases are based on main group metals) see: b) Y.-Q. Zheng, Z.-P. Kong, J.-L. Lin, *Z. Kristallogr. - New Cryst. Struct.* **2001**, *216*, 355–356; c) V. V. Sharutin, O. K. Sharutina, A. P. Pakusina, V. K. Belsky, *J. Organomet. Chem.* **1997**, *536*, 87–92.

[16] For unidentate coordination of fum dianion see: a) K. L. Zhang, Z. Wang, H. Huang, Y. Zhu, X. Z. You, *J. Mol. Struct.* **2004**, *693*, 193–197. For unidentate coordination of mal dianion see: b) Y.-Q. Zheng, J.-L. Lin, Z.-P. Kong, B.-Y. Chen, *J. Chem. Crystallogr.* **2002**, *32*, 399–408; c) C.-G. Zhang, Y.-J. Leng, Z.-F. Ma, D.-Y. Yan, *J. Chem. Crystallogr.* **1999**, *29*, 1081–1084.

[17] M. Du, X.-J. Zhao, *J. Mol. Struct.* **2003**, *655*, 191–197.

[18] Computation of the channel space is performed using PLATON program, see: A. L. Spek, *J. Appl. Crystallogr.* **2003**, *36*, 7–13.

[19] G. S. Rushbrooke, P. Wood, *Mol. Phys.* **1963**, *6*, 409–421.

[20] O. Kahn, *Molecular Magnetism*, VCH Publishers, New York, **1993**.

[21] C. Y. Weng, Ph. D. Thesis, Carnegie Institute of Technology, **1968**.

[22] a) F. D. M. Haldane, *Phys. Rev. Lett.* **1983**, *50*, 1153–1156; b) F. D. M. Haldane, *Phys. Lett. A* **1983**, *93*, 464–468; c) J. P. Renard, M. Verdaguer, L. P. Regnault, W. A. C. Erkelens, J. Rossat-Mignon, W. G. Stirling, *Europhys. Lett.* **1987**, *3*, 945–951; d) J. P. Renard, M. Verdaguer, L. P. Regnault, W. A. C. Erkelens, J. Rossat-Mignon, J. Ribas, W. G. Stirling, C. J. Vettier, *Appl. Phys.* **1988**, *63*, 3538–3542.

[23] R. Boca, *Coord. Chem. Rev.* **2004**, *248*, 757–815 and references cited therein.

[24] F. Bentiss, M. Lagrenee, *J. Heterocycl. Chem.* **1999**, *36*, 1029–1032.

[25] Bruker AXS, *SAINT Software Reference Manual*, Madison, WI, **1998**.

[26] G. M. Sheldrick, *SHELXTL NT Version 5.1. Program for Solution and Refinement of Crystal Structures*, University of Göttingen, Germany, **1997**.

Received: September 15, 2005
Published Online: January 26, 2006

